Article

Drug-Releasing Tannic Acid-Mediated Adhesive PEG Hydrogel for Porous Titanium Implants

Theeraporn Bubpamala, Patcharapit Promoppatum, and Pitirat Pholpabu*

Cite This: *ACS Omega* 2024, 9, 887−895

Read Online

ACCESS | Metrics & More | Article Recommendations | Supporting Information

ABSTRACT: Porous titanium implants are commonly utilized for orthopedic surgery because they can mimic the mechanical properties and porous structure of human bone. However, the bioinertness of titanium (Ti) has been reported to obstruct biointegration processes, resulting in slower bone repair. Here, we propose a localized drug delivery system on Ti surfaces using adhesive hydrogel to enhance biological-Ti interactions. The hydrogel was fabricated from polyethylene glycol (PEG), which was cross-linked by the complex of tannic acid (TA) and 1,4-phenylenediboronic acid (PDBA) and stabilized by bovine serum albumin (BSA). The hydrogel was formed and attached to a Ti plate to investigate stability, biodegradability, controlled drug release, and biocompatibility. The stability and biodegradability of the hydrogel could be tuned by adjusting the concentrations of BSA and TA. The hydrogel lasted and remained adhered to the Ti surface after being submerged in PBS for at least 15 days. The controlled release of strontium ranelate (SrRan) and the release mechanism depended on the amount of TA since it was found to govern the hydrogel integrity and pore size. Additionally, in vitro biocompatibility was validated using L929 fibroblast and MC3T3-E1 osteoblast cells that showed greater than 70% viability. The adhesive hydrogel was further studied by injecting it into a 3D-printed Ti-scaffold that contained a porous structure mimicking natural human bone. The hydrogel completely filled and adhered to the inner porous structure of the scaffold. The biodegradation and drug release of the hydrogel in the scaffold occurred at a slower rate, suggesting sustainable drug release that is suitable for bone cell regeneration. The overall results in biodegradability, controlled drug release, and biocompatibility demonstrate the great potential of the drug-releasing TA-mediated adhesive PEG hydrogel as a Ti-enhancing biomaterial that supports osseointegration.
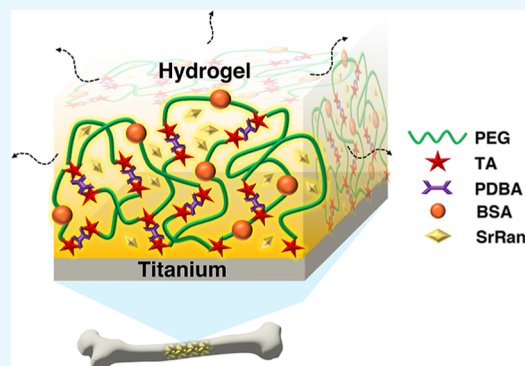
INTRODUCTION

Local drug delivery from hydrogel coatings is an advanced biomaterial strategy that can help enhance biological-metal interactions[1,2] and increase the clinical efficacy of metal implants.[3,4] Hydrogel that adheres to metal-based materials can potentially provide a tissue-mimicking microenvironment and a three-dimensional porous network for controlled drug release. In bone regenerative medicine, titanium (Ti) is the gold standard material for bone function restoration and has been developed with drug-releasing hydrogel coatings to achieve various biological purposes, including microbial reduction[5] and promotion of bone-related cell regeneration.[6,7] Nonetheless, hydrogel coatings on Ti typically erode relatively quickly for osseointegration processes that take longer than 14 days after implantation.[8,9] A drug-releasing hydrogel coating for bone integration is then suggested to have relatively high stability and slow degradation to provide longer and more sustainable drug release over the biointegration phases.[10]

Tannic acid (TA) is a natural derivative of polyphenolic compounds that can simultaneously form multiple chemical bonds to surrounding substances by catechol and pyrogallol groups residing in one single TA molecule.[11] The benefits of such multiple linkages include helping to cross-link polymers

to construct a hydrogel as well as creating gel adhesion to a substrate, thereby forming a hydrogel coating layer that can be fine-tuned for different medical requirements.[12,13] TA has received more attention in recent years for drug-releasing biomaterial development because of its strong intermolecular linkages that can last up to 14 days in a wet environment,[14] while the molecules essentially degrade by hydrolysis to noncytotoxic residues.[14] TA has shown many beneficial biological characteristics that are antioxidant, antibacterial, anticarcinogenic, and anti-inflammatory.[15,16] TA is recognized as a highly beneficial material component for orthopedic transplantation since it can suppress osteoclast activities and immobilize Sr (II) on Ti surface to enhance bone cell regeneration.[17] Our previous research demonstrates that TA can cross-link polyethylene glycol (PEG) to rapidly form a
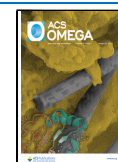
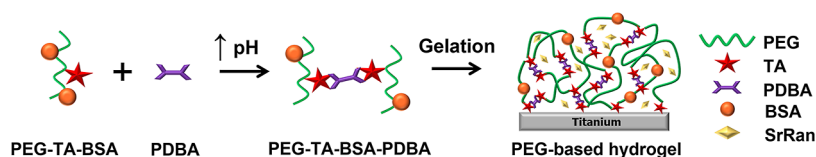**Scheme 1. Interactions of the Hydrogel Components on the Ti Substrate**

drug-releasing hydrogel after injection, providing a controlled release up to 25 days,[18] which is suggested to be sufficiently long for more proficient treatment of cancer cells.[19] However, we found that TA alone cannot cross-link PEG to form an adhesive hydrogel for a Ti coating. Another cross-linking system based on TA with greater stability and predictability can be achieved by creating dynamic boronate ester bonds that occur between TA and 1,4-phenylenediboronic acid (PDBA).[20] Under physiological conditions, the system can facilely and spontaneously cross-link polymers, such as PEG,[21] *O*-carboxymethyl chitosan (CMCS),[12] and hyaluronic acid (HA),[22] to construct self-healing hydrogels that have been reported to have minimal or negligible occurrences of adverse side effects.[23] Besides the beneficial TA bioactivities, these hydrogels have not yet been studied in relation to controlled drug release, which has the potential to greatly enhance the osseointegration of Ti.

In this study, TA-mediated PEG hydrogels were fabricated on Ti substrate as a coating layer and assessed for biodegradability to determine the hydrogel stability for controlled drug release. The FTIR analysis was used to confirm the interactions of the hydrogel components. For the controlled drug release study, strontium ranelate (SrRan)—an antiosteoporotic drug that rebalances bone remodeling through antiresorptive action and induces new bone formation—was selected as a drug model because local controlled release of SrRan from a hydrogel potentially reduces drug side effects, such as the risk of cardiac disease and poor bone mineralization in dialyzed patients.[24] The drug-loaded hydrogel was analyzed by SEM-EDS to confirm the presence of SrRan molecules in the porous network. The release mechanism of SrRan from the hydrogel coating was described by the Korsmeyer–Peppas model. A cytotoxicity study was also performed using L929 and MC3T3-E1 cell lines to determine the in vitro biocompatibility of the hydrogel. Last, the hydrogel was formed inside a 3D-printed Ti scaffold that mimics the structure of cancellous bone to investigate the drug release characteristics.

RESULTS AND DISCUSSION

Hydrogel Formation. Adhesive hydrogels were successfully synthesized into a coating layer on the Ti plate surface shortly after simultaneously injecting the pregel solution with NaOH. The chemical interactions among the hydrogel components and Ti are concisely depicted in Scheme 1. Our previous study showed that hydrogen bonds can occur between the ether groups of the PEG polymer and the catechol groups of TA and are primarily responsible for the interaction between PEG and TA.[18] The rapid formation of the hydrogel, which can be observed by the change in color from light yellow to red-orange, basically proves that the catechol groups in TA also bound the boronic acid in PDBA by the dynamic boronate ester bonds to generate a cross-linking point that occurred immediately after the solution pH was equal to or greater than the pK_a of the boronic acid.[12] The

FTIR results also confirm the interactions between PEG, TA, BSA, and PDBA in the hydrogel. As shown in Figure 1, it was
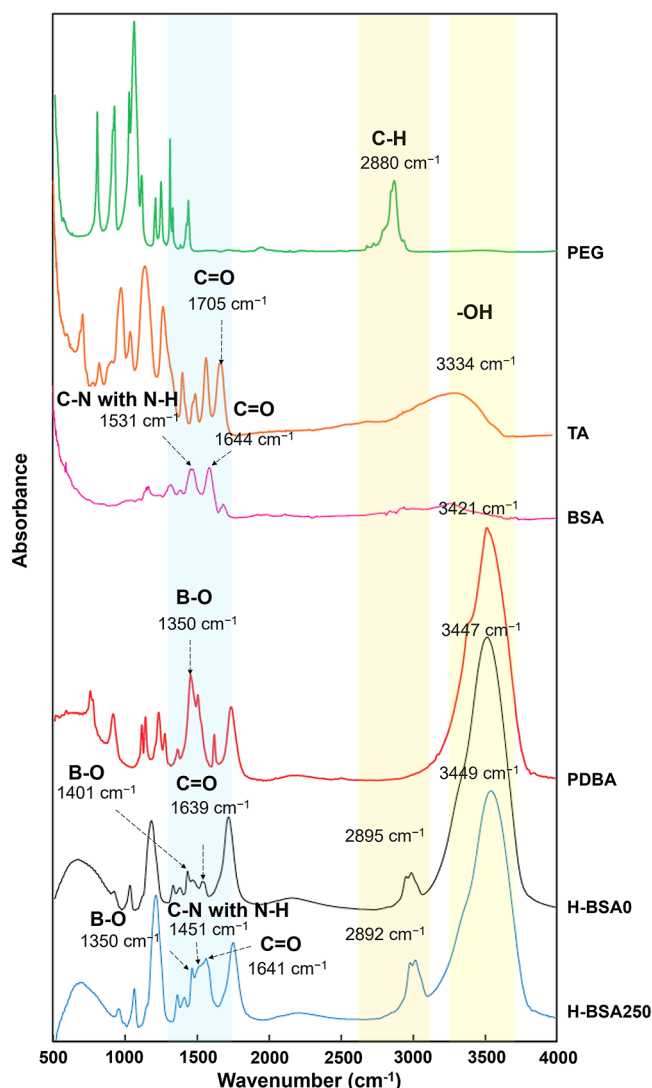

Figure 1. FTIR spectra of PEG, TA, PDBA, BSA, H-BSA0, and H-BSA250.

clearly seen that the strength of free −OH of TA (3334 cm^{-1}) and PDBA (3421 cm^{-1}) occurred in the spectra of H-BSA0 and H-BSA250 at 3447 and 3449 cm^{-1}, respectively. The C−H stretching of PEG attributed to hydrogel formation occurred and shifted from 2880 to 2895 cm^{-1} and 2892 cm^{-1} for H-BSA0 and H-BSA250, respectively. For H-BSA250, PEG and BSA interacted with amides I and II, where the peaks shifted from 1644 and 1531 cm^{-1} (C−N stretching coupled with N−H bending mode) to 1641 and 1451 cm^{-1}, respectively, similar to our previous study.[18] The peak ascribed to C═O vibration in TA (1705 cm^{-1}) shifted to 1639 and 1641 cm^{-1} for H-BSA0

and H-BSA250, respectively. Furthermore, the B−O stretching vibration of PDBA (1350 cm^{-1}) appeared in the spectra of H-BSA0 and H-BSA250 at 1401 and 1350 cm^{-1}, respectively, as a result of binding between the *cis*-diol moiety of TA to phenylboronic acid of PDBA.

Biodegradability. *Influence of BSA.* Similar to previous research, BSA was found to have a crucial role in stabilizing PEG hydrogels.[18,25] The formation of H-BSA0 showed that the interactions of PEG, TA, and PDBA still occurred even without BSA, but the hydrogel almost entirely degraded in just 1 day, as shown in Figure 2A. In contrast, the biodegradability
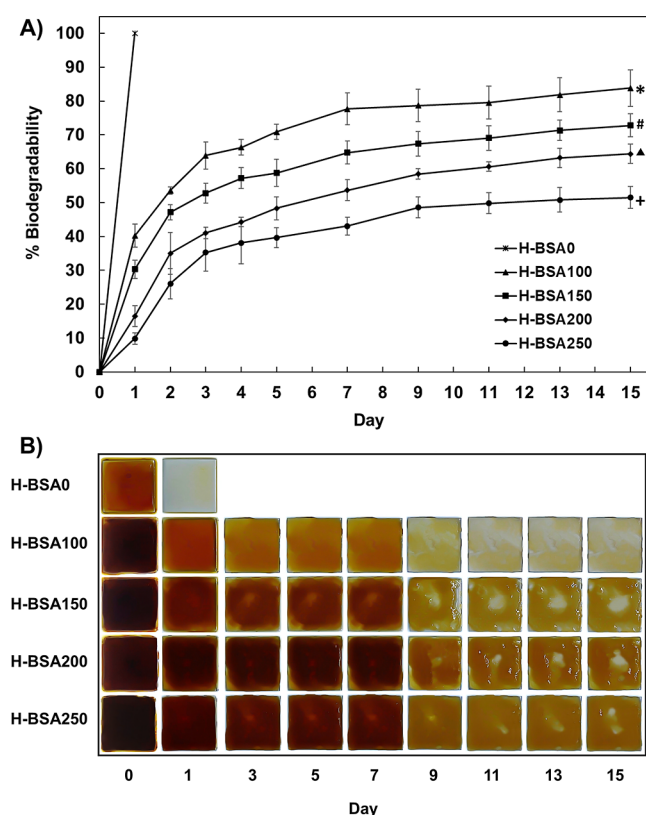
within pockets of the BSA molecule, and the PEG chain length is a critical factor in enhancing such hydrophobic interactions.[28] The longer chain leads to stronger binding and higher hydrogel stability.[28] Since the PEG used in the present study has a relatively high molecular weight (Mn) of 20,000, BSA is considered to be an important component to control hydrogel stability. Here, we chose to use the highest BSA concentration at 250 mg/mL for further studies.

Influence of TA. Like BSA, higher amounts of TA resulted in slower biodegradation of the hydrogel, as shown in Figure 3.
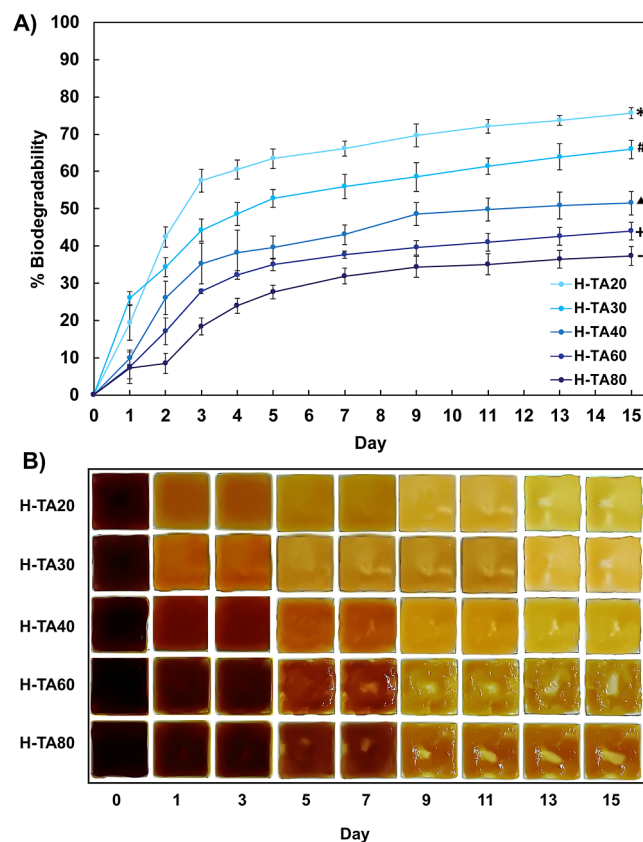
Figure 2. Effect of BSA on hydrogel biodegradability. (A) Biodegradability percentages of the hydrogels formed with the different BSA concentrations in PBS, pH 7.4 at 37 °C. The symbols at the end indicate significant difference from the repeated measures ANOVA with Conover post hoc pairwise analysis ($n = 3$). (B) Top-view appearance of the hydrogels.

Figure 3. Effect of TA on the hydrogel biodegradability. (A) Biodegradability percentages of the hydrogels formed with different TA concentrations in PBS, pH 7.4 at 37 °C. The symbols at the end indicate significant difference from the repeated measures ANOVA with Conover post hoc pairwise analysis ($n = 3$). (B) Top-view appearances of the hydrogels.

of the hydrogels became much slower when BSA was added. The amounts of BSA were found to be statistically significant in reducing the degradation rate. In 15 days, the biodegradability percentages of H-BSA100, H-BSA150, H-BSA200, and H-BSA250, became 84 ± 5.4, 73 ± 3.4, 64 ± 2.8, and 51 ± 3.2, respectively, suggesting that all of the BSA-stabilized hydrogels can be used as Ti coatings for new bone development that approximately takes 14 days.[26] The appearance of the hydrogels that correspond with the decreasing percentage of biodegradability is shown in Figure 2B. The distinct hydrogel colors depict the different amounts of the borate−catechol complexes that decreased following the hydrogel degradation.[27] The maximum concentration of BSA was 250 mg/mL for the study because of the limited solubility of BSA. The enhanced stability of the hydrogel can be described by the hydrophobic interactions that occur between PEG and BSA

Immersed in PBS at 37 °C for 15 days, H-TA20, H-TA30, H-TA40, H-TA60, and H-TA80 showed significantly different degradation percentages over time and reached 76 ± 1.5, 66 ± 2.5, 51 ± 3.2, 44 ± 2.4, and 37 ± 2.5, respectively, at the end of the experiment. In this study, we used the maximum TA concentration of 80 mg/mL because the higher TA concentration turned the mixture into a coacervation phase. Here, TA is a very important component to form the adhesive hydrogel because it links the polymer chains in addition to the polymer chains and the Ti substrate. TA binds to PDBA via dynamic boronate ester bonds that create a stable linkage complex.[29] The hydrogel with the lower amount of TA contains a limited number of cross-linking complexes, resulting in looser polymeric networks that presumably result in a faster degradation rate and drug release on the Ti surface. Regarding chemical structure, one PDBA molecule can bind with two TA
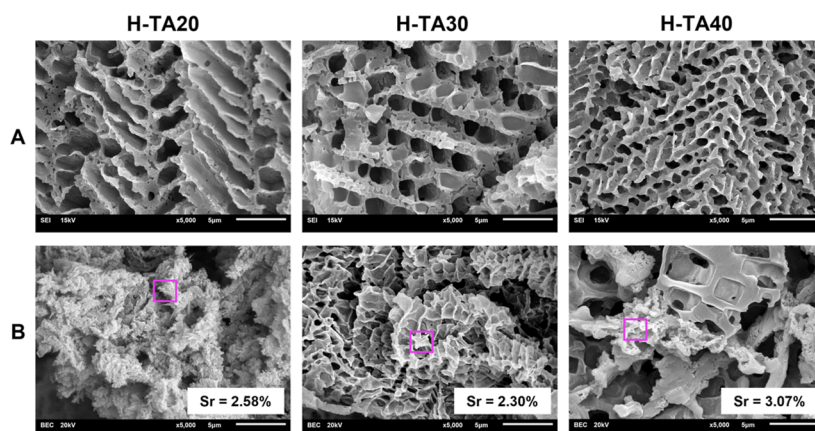
Figure 4. SEM-EDS characterization of the SrRan-encapsulated hydrogels, H-TA20, H-TA30, and H-TA40. (A) SEM micrographs showing the hydrogel porous structures. (B) EDS analysis of Sr in the hydrogel. The pink box represents the EDS scanning area.

molecules, so it is reasonable that H-TA20, H-TA30, H-TA40, and H-TA60, which contain increasing TA/PDBA molar ratios of 0.7:1, 1:1, 1.3:1, and 2:1, respectively, would result in slower degradation. It is interesting that H-TA80, which had a 2.7:1 TA/PDBA molar ratio, still resulted in significantly slower degradation than H-TA60 with a 2:1 molar ratio. This phenomenon might be caused by an increased possibility of TA-PDBA complex formation or TA-polymer binding. The effect of the TA concentration was then further investigated for controlled drug release.

Controlled Drug Release. The drug-loaded hydrogels with different amounts of TA were studied by SEM-EDS to investigate the hydrogel porous structure and the encapsulated drug particle. As shown in Figure 4A, more TA resulted in a denser porous matrix of the hydrogel. The micropores in H-TA20, H-TA30, and H-TA40 were 3.12 ± 0.28, 2.22 ± 0.12, and 1.08 ± 0.08 μm in diameter, respectively. The measured pore size agrees with biodegradability results, in which the smaller micropores provided a dense polymeric network, resulting in hydrogels that biodegraded slower than larger micropores. The presence of strontium (Sr) element from EDS analysis verifies that SrRan particles were captured inside the hydrogel (Figure 4B), and some were also attached on the outer surface (Figure S1). The dispersion of Sr in the hydrogel is shown in the elemental mapping (Figure S2). The percentages of Sr elements in H-TA20, H-TA30, and H-TA40 were 2.58, 2.30, and 3.07%, respectively. The drug particles were 11.19 ± 0.87 μm in diameter, larger than the hydrogel micropore for all TA variations. Such relatively smaller pores suggest that the drug release is likely dependent upon hydrogel erosion rather than diffusion.

To further analyze the controlled drug release, the drug release profiles of the hydrogels formed with varied TA concentrations were periodically recorded for 15 days. As shown in Figure 5, the drug release profiles depend on the TA amount. Higher amounts of TA significantly decelerate the drug release in a similar manner to biodegradation. The results suggest that the drug release directly relates to the different numbers of the TA-PDBA cross-linking complex. H-TA20, which has the lowest TA/PDBA molar ratio, contains minimal TA molecules that limit the formation of the cross-linking complex, leading to a looser polymeric network that permeates more water, degrades faster, and consequently allows SrRan to come out more rapidly. The drug release mechanism was also determined by fitting the curve to the Korsmeyer–Peppas
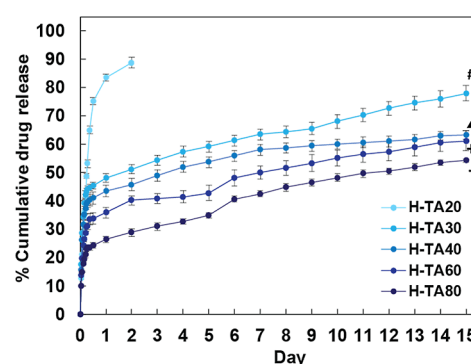

Figure 5. Release profiles of SrRan from the adhesive hydrogels synthesized with different TA concentrations on a Ti plate. The symbols at the end indicate the significant difference from the repeated measures ANOVA with Conover post hoc pairwise analysis ($n = 3$).

model (Figure S3) in eq 1, which is applicable to less than 60% of the release curve.[30,31]

$$F = kt^n \qquad (1)$$

where F is the fraction of the drug released at time t, k is drug diffusion coefficient, and n is the release exponent that indicates the release mechanism of small molecules from a polymer matrix. A value of $n < 0.5$ indicates a pseudo-Fickian behavior of diffusion where release curves resemble Fickian diffusion but the releasing rate is very slow, while $n = 0.5$ indicates Fickian or Case I transport behavior. $0.5 < n < 1$ indicates an anomalous transport process, which corresponds to Case III and the structural relaxation. $n = 1$ indicates a non-Fickian or Case II mode of transport.[32−34] As expected, the fitted n, shown in Table S1, indicates that the amount of TA affects the release mechanism, and two mechanisms are identified. The values of n for H-TA20, H-TA30, H-TA40, H-TA60, and H-TA80 are 0.51 ± 0.01, 0.22 ± 0.01, 0.22 ± 0.01, 0.24 ± 0.02, and 0.23 ± 0.01, respectively, indicating that only H-TA20 demonstrated Fickian diffusion, while the other hydrogels performed pseudo-Fickian diffusion. It is interesting that even though H-TA20 contained much smaller pores (3.12 ± 0.28 μm) than the drug particles (11.19 ± 0.87 μm), the release followed Fickian diffusion. This occurrence might be explained by the loose polymeric network or the rapid hydrogel degradation that coincided with the diffusion rate.
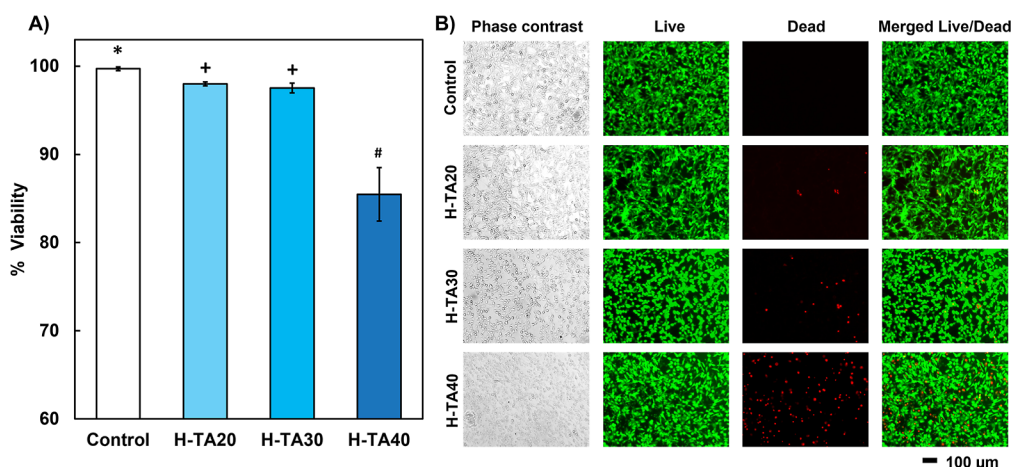
Figure 6. (A) Cell viabilities of L929 mouse fibroblast cells incubated with H-TA20, H-TA30, and H-TA40 for 24 h. DMEM was used as the negative control. The symbols at the top indicate significant difference from the Kruskal–Wallis test with Conover post hoc pairwise analysis ($n = 3$). (B) Micrographs of the cells. Live and dead cells are shown in green and red, respectively.

Figure 7. (A) Cell viabilities of MC3T3-E1 mouse osteoblast cells incubated with H-TA20, H-TA30, and H-TA40, for 24 h. MEMα was used as the negative control. The symbols at the top indicate significant difference from the Kruskal–Wallis test with Conover post hoc pairwise analysis ($n = 3$). (B) Micrographs of the cells. Live and dead cells are shown in green and red, respectively.
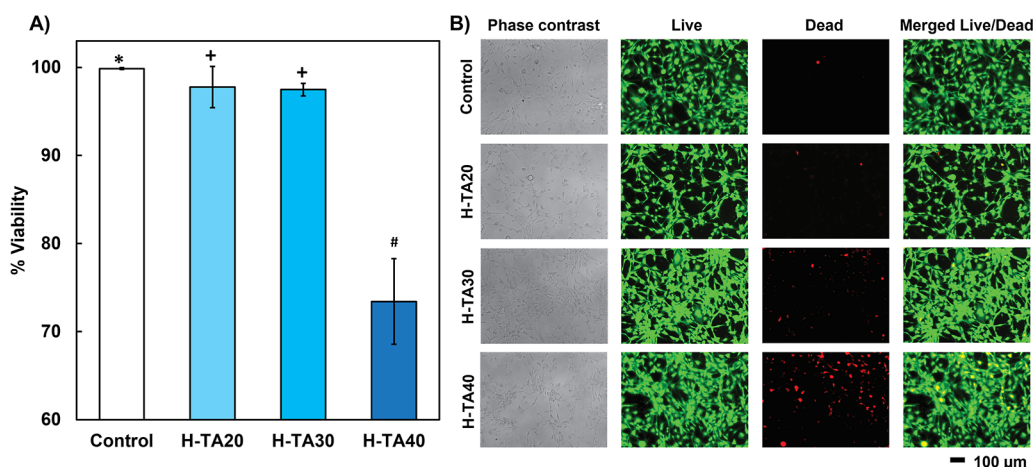
Meanwhile, hydrogels that contained higher amounts of TA exhibited a stronger and denser matrix and released the drug at a much slower rate, suggesting that erosion was involved. Regarding release profiles, drug release can be considered to have two separate stages of release mechanisms. The early stage occurred within about 3 days, in which SrRan was mainly released from diffusion but partially decelerated by the dense matrix. However, the matrix degraded at a relatively fast rate. Therefore, the release profiles are similar to Fickian diffusion but slower. For the late stage, the release profiles are considered to have a steady slope that is similar to biodegradation, implying that the drug release mostly relied on the degradability of the hydrogel. Moreover, the drug diffusion coefficient (k) of hydrogel was found to have lower values when increasing TA concentration. The k values of H-TA20, H-TA30, H-TA40, H-TA60, and H-TA80 are 94.58, 53.90, 48.63, 39.80, and 27.74, respectively, which corresponded to the drug release profile and suggested that the drug-loaded hydrogels with a large amount of TA resulted in a slow release. Effective controlled release of SrRan is beneficial to drug administration because SrRan has a limited range of biocompatible concentrations with osteoblast cells (0.1–12

mM).[24] The fine-tuned drug release profile through an adjustable concentration of TA presented in this hydrogel is then preferable for a controlled delivery system of SrRan. The results of these findings suggest that hydrogel is an appropriate option for delivering SrRan in order to effectively regulate and enhance the process of osteoblast cell regeneration on the surface of Ti.

Biocompatibility. The adhesive hydrogels formed with different TA concentrations showed significantly different levels of cytotoxicity that can be observed by both L929 and MC3T3-E1 cell viabilities, as shown in Figures 6 and 7, respectively. For H-TA20 and H-TA30, the hydrogels had similarly negligible cytotoxicity at more than 90% cell viability for both types of cells. The hydrogels formed with TA concentrations higher than 30 mg/mL were found to cause significantly higher cytotoxic levels. H-TA40 had percentages of viability of 85.5 ± 3.0% for L929 and 73.0 ± 5.0% for MC3T3-E1, which might still be considered as biocompatible with the cells with regard to the ISO Standard 10993-5 that states that a material is cytotoxic when cell viability is found to be less than 70%.[35] In contrast, H-TA60 and H-TA80 resulted in very high cytotoxicity, which caused the cells to detach from
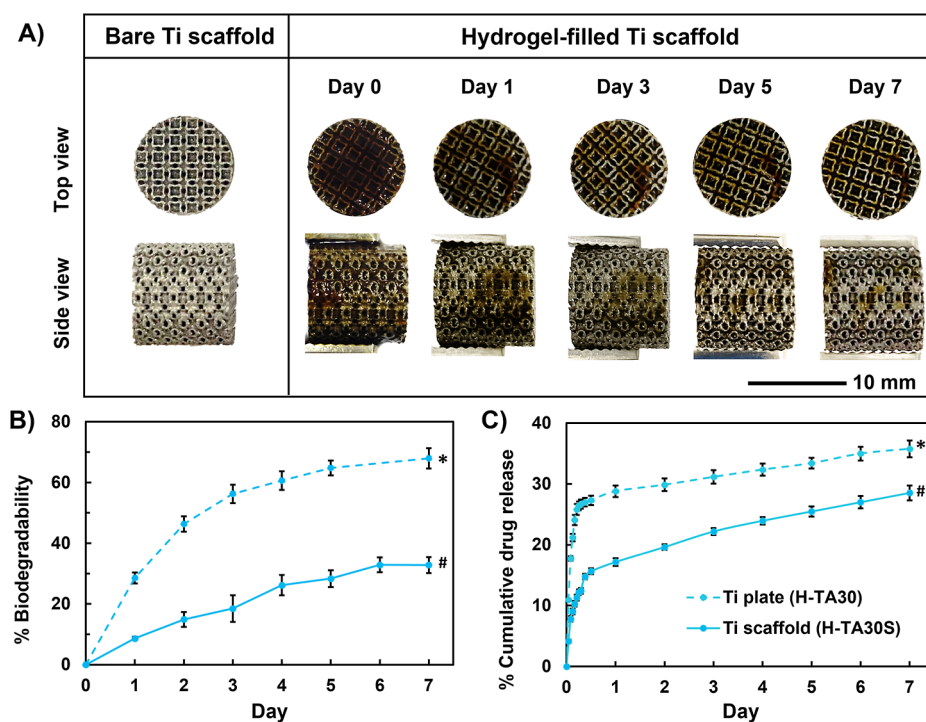
Figure 8. Adhesive hydrogel in the 3D-printed Ti scaffold. (A) Top and side views of the Ti scaffolds filled with hydrogel and kept in PBS, pH 7.4 at 37 °C. (B) Percentages of the biodegradability of H-TA30S compared with H-TA30. (C) Drug release profiles of H-TA30S compared with H-TA30. The symbols at the end indicate significant difference from the repeated measures ANOVA with Conover post hoc pairwise analysis ($n = 3$).

the culture surface. The results illustrate that the amount of TA not only dictates the drug release profile and mechanism but also affects the biocompatibility of the hydrogel. H-TA30 provided the highest biocompatibility and longest sustained drug release so it was chosen for further investigation with the 3D-printed Ti scaffold.

Adhesive Hydrogel in 3D-Printed Ti Scaffold. The adhesive hydrogel in the Ti scaffold (H-TA30S) was comparable to the hydrogel coated on the Ti plate (H-TA30) in terms of gelation time and appearance, but the biodegradability and the drug release were significantly different. Shortly after injecting the hydrogel components into the Ti scaffold, the hydrogel rapidly formed inside the void and was well attached to the metal structure, as shown in Figure 8A. The hydrogel color was similar to H-TA30 (Figure 3B) as expected since the hydrogel precursors contained the exact same components. The hydrogel adhered and remained in the Ti scaffold for at least 7 days. As shown in Figure 8B, H-TA30S gradually degraded, and on day 7, the hydrogel mass reduced by $32.8 \pm 0.6\%$, which was about 2-fold less than H-TA30 ($68.0 \pm 3.3\%$). For the drug release, Figure 8C demonstrates that the cumulative percentage of the released SrRan from H-TA30S was also much less than H-TA30. Similar to H-TA30, the drug release from H-TA30S can be divided into two stages. For the early stage, the release profile shape was comparable to H-TA30 with a much slower rate, while after that, the release rate became approximately constant for both of the hydrogels. As mentioned above, the two-stage drug release can be explained by the hydrogel biodegradation that became the main limiting factor for the late period. The differences in biodegradability and drug release profiles between H-TA30 and H-TA30S can additionally be described by the surface area to volume (SA/V) ratio. H-TA30S has a smaller SA/V ratio of 0.6 mm^{-1} compared to

H-TA30 at 0.8 mm^{-1}, meaning that H-TA30S has relatively less surface area to contact with the aqueous surroundings. It is therefore reasonable that the biodegradation and the drug release of H-TA30S occurred at a slower rate than H-TA30. The overall result suggests that our adhesive hydrogel is versatile, can be coated on different shapes of Ti, and provides controlled drug release without significant cytotoxicity. Moreover, besides Schoen's I-graph-Wrapped Package (IWP), which was used in this study, there are other triply periodic minimal surface porous structures that have been reported to have applicability as bone substitute structures, such as primitive, gyroid, diamond, and neovius.[36] The advantages of the porous patterns in the 3D-printed Ti implants combined with the controlled drug release from the tannic acid-mediated adhesive PEG hydrogel would be of interest to accelerate bone cell regeneration.

■ CONCLUSIONS

In this study, a tannic acid-mediated adhesive PEG hydrogel was successfully constructed on a flat Ti plate and in a porous 3D-printed Ti scaffold to control SrRan release. The stability and biodegradability of the hydrogels could be modified by adjusting the BSA and TA concentrations to correspond with the Ti-bone integration timeline. The drug release mechanisms of the hydrogel were explained via the Korsmeyer–Peppas model, in which the hydrogel released the drug through diffusion and erosion processes. The SEM-EDS analysis results revealed the hydrogel porous morphology and the encapsulated SrRan particles. H-TA20, H-TA30, and H-TA40 exhibited excellent in vitro biocompatibility with both L929 mouse fibroblasts and MC3T3-E1 mouse osteoblasts. The adhesive hydrogel can be both utilized as a Ti-plate coating and a 3D-printed Ti-scaffold filling for controlled drug release. According to the results, the tannic acid-mediated adhesive

PEG hydrogels have shown high potential as a Ti-adhesive biomaterial that could enhance osseointegration by controlled drug release.

■ EXPERIMENTAL SECTION

Materials. Poly(ethylene glycol) (PEG, M_n = 20,000 g/mol) was purchased from Sigma-Aldrich Chemical Inc. (USA). Tannic acid (TA, reagent) and phosphate-buffered saline (PBS, 0.01 M, pH 7.4) were purchased from Alfa Aesar (United Kingdom). 1,4-Phenylenediboronic acid (PDBA, $C_6H_8B_2O_4$, M_n = 165.75 g/mol) and strontium ranelate (SrRan, $C_{12}H_6N_2O_8SSr_2 \cdot xH_2O$, M_n = 513.49 g/mol) were purchased from Tokyo Chemical Industry (Japan). Sodium hydroxide (NaOH) was purchased from Merck Inc. (Germany). Dulbecco's modified Eagle medium (DMEM; Gibco), fetal bovine serum (FBS; Gibco), and penicillin–streptomycin were purchased from Thermo Fisher Scientific Inc. (USA). Minimal essential medium alpha (MEM α; HyClone) was purchased from Cytiva (USA). Sterile flat-bottom 24-well plates and transwell inserts (pore size 0.8 μm) were purchased from Corning Inc. (USA). All aqueous solutions were prepared using distilled water. Titanium plate (grade 5, size 20 × 20 × 1 mm) was purchased from Prolog Titanium Corporation (Thailand). Titanium powder (grade 5) was purchased from TRUMPF Inc. (Germany).

Adhesive Hydrogel Formation on a Ti Plate. Fabrication of the TA-mediated PEG hydrogel coating on Ti was achieved through a one-pot formation process. To prepare 1 mL of the pregel mixture, 0.5 mL of PEG (the final concentration of 0.05 M), TA, and BSA (when required) were vortex mixed. The weight and final concentrations of TA and BSA are summarized in Table 1. To investigate the controlled

Table 1. Concentrations of BSA and TA in the Hydrogels

hydrogels	BSA (mg)	TA (mg)
H-BSA0		40
H-BSA100	100 (1.50 mM)	40
H-BSA150	150 (2.25 mM)	40
H-BSA200	200 (3.00 mM)	40
H-BSA250	250 (3.76 mM)	40
H-TA20	250	20 (50 mM)
H-TA30	250	30 (70 mM)
H-TA40	250	40 (90 mM)
H-TA60	250	60 (140 mM)
H-TA80	250	80 (190 mM)

drug release, SrRan was added to reach a final concentration of 5.84 mM. Next, 0.75 mL of the mixture was combined with 0.25 mL of PDBA (the final concentration of 0.07 M) and stirred until homogeneous. The total 1 mL of pregel solution was last coinjected with 0.03 M NaOH to adjust pH right on a grade 5 titanium plate. The mixture was spontaneously spread out over the Ti plate and formed into an adhesive layer of hydrogel. The hydrogel was then kept in PBS at room temperature and characterized within 30 min.

FTIR Analysis. The hydrogels with and without BSA were plunged into liquid nitrogen to instantaneously freeze the hydrogel structural features. The hydrogels were then freeze-dried for 2 days and ground into a rough powder. The infrared spectrum was measured using a Fourier transform infrared spectrometer (Thermo Scientific Nicolet iS5 FTIR spectrometer) in the range of 4000−550 cm^{-1}.

Biodegradability. All hydrogels were assessed for biodegradability. The biodegradability percentage of the hydrogel was determined using eq 2.[37] Immediately after preparation of the hydrogel coating on a Ti plate, the hydrogel was completely dried to obtain the initial weight (W_i). The hydrogels were also additionally prepared, incubated in PBS at 37 °C, pH 7.4, for different designated time periods over 15 days, and dried to measure the dried weight (W_d) at the specific time points.

$$\text{biodegradability (\%)} = \frac{W_i - W_d}{W_i} \times 100 \tag{2}$$

SEM-EDS Analysis. The hydrogel morphology and encapsulation of H-TA20, H-TA30, and H-TA40 were analyzed by SEM-EDS. The hydrogels were promptly immersed and frozen in liquid nitrogen after preparation. Two-day freeze-drying was then conducted to achieve complete dehydration. Sputter coating with gold was performed in the Cressington 108 Auto instrument onto the freeze-dried hydrogel to increase the signal-to-noise ratio for SEM imaging. The surface and cross-sectional morphology of the hydrogel were examined using a scanning electron microscope JSM-6610 LV (JEOL worldwide, India). Energy dispersive X-ray spectroscopy (OXFORD, INCAx-act) was also performed to analyze the SrRan drug encapsulation and dispersion in the hydrogel.

Drug Release Study. Drug releases from the hydrogels with the varied amounts of TA were investigated. Briefly, the hydrogel was prepared on a Ti plate and incubated to release the drug in 4 mL of PBS at 37 °C. The solution was collected and replaced with fresh PBS at different designated time points for up to 15 days. Drug concentration was determined by fluorescent absorbance at 320 nm[38] using a Multiskan SkyHigh microplate spectrophotometer (Thermo Scientific, USA). The drug release mechanism of the hydrogel coating was analyzed by fitting experimental data (24 h for H-TA20 and 3 days for H-TA30, H-TA40, H-TA60, and H-TA80) to the drug release model Korsmeyer−Peppas[30,31] with the DDSolver add-in program in MS Excel.[39]

Cytotoxicity Test. Cytotoxicity of the material was assessed using L929 mouse fibroblasts (ATCC, Manassas, VA), in accordance with the ISO Standard 10993-5,[35] and MC3T3-E1 mouse osteoblasts because of the potential use in orthopedic applications. L929 cells were cultured in DMEM (MEM α for MC3T3-E1) supplemented with 10% FBS and 1% penicillin/streptomycin in a 24-well plate. When the cells achieved approximately 80% confluence, a transwell insert was then placed at the top of each well and injected with 0.2 mL hydrogel precursors inside the inset to perform an indirect contact cytotoxicity assessment of the hydrogels with the different amounts of TA— H-TA20, H-TA30, H-TA40, H-TA60, and H-TA80.[18] Subsequently, the cells and the hydrogels were incubated together at 37 °C with 5% CO$_2$ for 24 h. The cell viability assessment was conducted using a Live/Dead Assay Kit (L-3224, Invitrogen, Life Technologies, Foster City, CA). The fluorescent-stained cells were imaged using Cytell Cell Imaging System by GE Healthcare Life Science and then analyzed using NIH ImageJ software, accessible at http://rsb.info.nih.gov/ij.

Preparation and Characterization of the Adhesive Hydrogel in Ti Scaffold. The drug-releasing hydrogel H-TA30 was further studied in the form of an adhesive filling in a

3D-printed Ti scaffold (H-TA30S). The scaffold was designed in a cylindrical 3D shape (Ø10 mm × H10 mm) containing the IWP porous structure, one of the skeletal-based structures, with a pore size of 0.85 mm and porosity of 78.7% (Figure S4) to mimic the internal structure of human cancellous bone.[40,41] 3D printing was performed in a laser powder bed fusion system (TruPrint 1000, TRUMPF Inc., Germany) by melting grade 5 Ti powder, printing the structure layer by layer, and solidifying it by cooling. The scaffold was then ultrasonically cleaned in acetone, ethyl alcohol, and deionized water for 15 min each and fitted into a 48-well plate. Next, the pregel mixtures of H-TA30S with SrRan and NaOH were simultaneously injected into the Ti scaffold to form the hydrogel. The hydrogel-filled Ti scaffold was then imaged, assessed for biodegradability, and the drug release over time was determined by conducting the same protocol mentioned above.

Statistical Analysis. All experiments were conducted in triplicate with the results reported as mean ± standard deviation. Statistical analysis was conducted using OriginPro 2022b (Learning Edition) software. The cytotoxicity test results were analyzed using the Kruskal–Wallis test because of the small sample size. The biodegradability percentage and drug release profile were analyzed using repeated measures ANOVA, followed by Conover's post hoc pairwise analysis. The threshold p-value of 0.05 was used to determine the statistical significance of the data.

■ ASSOCIATED CONTENT

ⓈI Supporting Information

The Supporting Information is available free of charge at https://pubs.acs.org/doi/10.1021/acsomega.3c06966.

> SEM micrograph of SrRan particles on the hydrogel surface; elemental mapping of the strontium (Sr) element dispersed in the hydrogel; curve fitting of the drug release profile to the Korsmeyer–Peppas model; Ti scaffold with IWP porous structure containing a pore size of 0.85 mm and porosity of 78.7%; IWP unit cell; measurement of the pore size designated as the longest diameter of a sphere that can fit into the pore; and R^2, drug diffusion coefficient (k), and shape parameter (n) calculated from the Korsmeyer–Peppas model (PDF)

■ AUTHOR INFORMATION

Corresponding Author

Pitirat Pholpabu − *Biological Engineering Program, Faculty of Engineering, King Mongkut's University of Technology Thonburi, Bangkok 10140, Thailand;* ⓞ orcid.org/0000-0002-4418-8872; Email: pitirat.pho@mail.kmutt.ac.th

Authors

Theeraporn Bubpamala − *Biological Engineering Program, Faculty of Engineering, King Mongkut's University of Technology Thonburi, Bangkok 10140, Thailand*

Patcharapit Promoppatum − *Department of Mechanical Engineering, Faculty of Engineering, King Mongkut's University of Technology Thonburi, Bangkok 10140, Thailand*

Complete contact information is available at:
https://pubs.acs.org/10.1021/acsomega.3c06966

Notes

The authors declare no competing financial interest.

■ ACKNOWLEDGMENTS

■ REFERENCES

(1) Yang, W. J.; Tao, X.; Zhao, T.; Weng, L.; Kang, E.-T.; Wang, L. Antifouling and Antibacterial Hydrogel Coatings with Self-Healing Properties Based on a Dynamic Disulfide Exchange Reaction. *Polym. Chem.* **2015**, *6* (39), 7027−7035.

(2) Zhang, B.; Li, J.; He, L.; Huang, H.; Weng, J. Bio-Surface Coated Titanium Scaffolds with Cancellous Bone-like Biomimetic Structure for Enhanced Bone Tissue Regeneration. *Acta Biomater.* **2020**, *114*, 431−448.

(3) Romanò, C. L.; Malizos, K.; Capuano, N.; Mezzoprete, R.; D'Arienzo, M.; Der, C. V.; Scarponi, S.; Drago, L. Does an Antibiotic-Loaded Hydrogel Coating Reduce Early Post-Surgical Infection After Joint Arthroplasty? *J. Bone Jt. Infect.* **2016**, *1*, 34−41.

(4) Malizos, K.; Blauth, M.; Danita, A.; Capuano, N.; Mezzoprete, R.; Logoluso, N.; Drago, L.; Romanò, C. L. Fast-Resorbable Antibiotic-Loaded Hydrogel Coating to Reduce Post-Surgical Infection after Internal Osteosynthesis: A Multicenter Randomized Controlled Trial. *J. Orthop. Traumatol.* **2017**, *18* (2), 159−169.

(5) Romanò, C.; Vecchi, E. D.; Bortolin, M.; Morelli, I.; Drago, L. Hyaluronic Acid and Its Composites as a Local Antimicrobial/Antiadhesive Barrier. *J. Bone Jt. Infect.* **2017**, *2* (1), 63−72.

(6) Wang, Y.; Feng, Z.; Liu, X.; Yang, C.; Gao, R.; Liu, W.; Ou-Yang, W.; Dong, A.; Zhang, C.; Huang, P.; Wang, W. Titanium Alloy Composited with Dual-Cytokine Releasing Polysaccharide Hydrogel to Enhance Osseointegration via Osteogenic and Macrophage Polarization Signaling Pathways. *Regenerative Biomaterials* **2022**, *9*, rbac003.

(7) Li, X.; Xu, K.; He, Y.; Tao, B.; Li, K.; Lin, C.; Hu, J.; Wu, J.; Wu, Y.; Liu, S.; Liu, P.; Wang, H.; Cai, K. ROS-Responsive Hydrogel Coating Modified Titanium Promotes Vascularization and Osteointe-gration of Bone Defects by Orchestrating Immunomodulation. *Biomaterials* **2022**, *287*, 121683.

(8) Mello-Machado, R. C.; Sartoretto, S. C.; Granjeiro, J. M.; Calasans-Maia, J. d. A.; de Uzeda, M. J. P. G.; Mourão, C. F. d. A. B.; Ghiraldini, B.; Bezerra, F. J. B.; Senna, P. M.; Calasans-Maia, M. D. Osseodensification Enables Bone Healing Chambers with Improved Low-Density Bone Site Primary Stability: An in Vivo Study. *Sci. Rep.* **2021**, *11* (1), 15436.

(9) Liu, Y.; Rath, B.; Tingart, M.; Eschweiler, J. Role of Implants Surface Modification in Osseointegration: A Systematic Review. *J. Biomed. Mater. Res., Part A* **2020**, *108* (3), 470−484.

(10) Agarwal, R.; García, A. J. Biomaterial Strategies for Engineering Implants for Enhanced Osseointegration and Bone Repair. *Adv. Drug Deliv. Rev.* **2015**, *94*, 53−62.

(11) Lu, R.; Zhang, X.; Cheng, X.; Zhang, Y.; Zan, X.; Zhang, L. Medical Applications Based on Supramolecular Self-Assembled Materials From Tannic Acid. *Front. Chem.* **2020**, *8*, 583484.

(12) Geng, H.; Dai, Q.; Sun, H.; Zhuang, L.; Song, A.; Caruso, F.; Hao, J.; Cui, J. Injectable and Sprayable Polyphenol-Based Hydrogels for Controlling Hemostasis. *ACS Appl. Bio Mater.* **2020**, *3* (2), 1258−1266.

(13) Chen, K.; Lin, Q.; Wang, L.; Zhuang, Z.; Zhang, Y.; Huang, D.; Wang, H. An All-in-One Tannic Acid-Containing Hydrogel Adhesive with High Toughness, Notch Insensitivity, Self-Healability, Tailorable Topography, and Strong, Instant, and On-Demand Underwater Adhesion. *ACS Appl. Mater. Interfaces* **2021**, *13* (8), 9748−9761.

(14) Jing, J.; Liang, S.; Yan, Y.; Tian, X.; Li, X. Fabrication of Hybrid Hydrogels from Silk Fibroin and Tannic Acid with Enhanced Gelation

and Antibacterial Activities. *ACS Biomater. Sci. Eng.* **2019**, *5* (9), 4601−4611.

(15) Ghasemian, M.; Kazeminava, F.; Naseri, A.; Mohebzadeh, S.; Abbaszadeh, M.; Kafil, H. S.; Ahmadian, Z. Recent Progress in Tannic Acid Based Approaches as a Natural Polyphenolic Biomaterial for Cancer Therapy: A Review. *Biomed. Pharmacother.* **2023**, *166*, 115328.

(16) He, H.; Qin, Q.; Xu, F.; Chen, Y.; Rao, S.; Wang, C.; Jiang, X.; Lu, X.; Xie, C. Oral Polyphenol-Armored Nanomedicine for Targeted Modulation of Gut Microbiota-Brain Interactions in Colitis. *Sci. Adv.* **2023**, *9* (21), No. eadf3887.

(17) Steffi, C.; Shi, Z.; Kong, C. H.; Chong, S. W.; Wang, D.; Wang, W. Use of Polyphenol Tannic Acid to Functionalize Titanium with Strontium for Enhancement of Osteoblast Differentiation and Reduction of Osteoclast Activity. *Polymers* **2019**, *11* (8), 1256.

(18) Bubpamala, T.; Viravaidya-Pasuwat, K.; Pholpabu, P. Injectable Poly(Ethylene Glycol) Hydrogels Cross-Linked by Metal-Phenolic Complex and Albumin for Controlled Drug Release. *ACS Omega* **2020**, *5* (31), 19437−19445.

(19) Johnson-Arbor, K.; Dubey, R. Doxorubicin. *StatPearls*; StatPearls Publishing: Treasure Island (FL), 2023;.

(20) Chen, C.; Yang, H.; Yang, X.; Ma, Q. Tannic Acid: A Crosslinker Leading to Versatile Functional Polymeric Networks: A Review. *RSC Adv.* **2022**, *12* (13), 7689−7711.

(21) Huang, Z.; Delparastan, P.; Burch, P.; Cheng, J.; Cao, Y.; Messersmith, P. B. Injectable Dynamic Covalent Hydrogels of Boronic Acid Polymers Cross-Linked by Bioactive Plant-Derived Polyphenols. *Biomater. Sci.* **2018**, *6* (9), 2487−2495.

(22) Montanari, E.; Gennari, A.; Pelliccia, M.; Gourmel, C.; Lallana, E.; Matricardi, P.; McBain, A. J.; Tirelli, N. Hyaluronan/Tannic Acid Nanoparticles Via Catechol/Boronate Complexation as a Smart Antibacterial System. *Macromol. Biosci.* **2016**, *16* (12), 1815−1823.

(23) Cambre, J. N.; Sumerlin, B. S. Biomedical Applications of Boronic Acid Polymers. *Polymer* **2011**, *52* (21), 4631−4643.

(24) Marx, D.; Rahimnejad Yazdi, A.; Papini, M.; Towler, M. A Review of the Latest Insights into the Mechanism of Action of Strontium in Bone. *Bone Reports* **2020**, *12*, 100273.

(25) Bubpamala, T.; Pholpabu, P. Mechanical Properties of Sprayable Poly(Ethylene Glycol) Hydrogels. *Proceedings of Pure and Applied Chemistry International Conference (PACCON 2019)*: Bangkok, 2019; pp PO1−PO4.

(26) Wang, Y.; Zhang, Y.; Miron, R. J. Health, Maintenance, and Recovery of Soft Tissues around Implants. *Clin. Implant Dent. Relat. Res.* **2016**, *18* (3), 618−634.

(27) He, L.; Fullenkamp, D. E.; Rivera, J. G.; Messersmith, P. B. pH Responsive Self-Healing Hydrogels Formed by Boronate-Catechol Complexation. *Chem. Commun.* **2011**, *47* (26), 7497−7499.

(28) Bekale, L.; Agudelo, D.; Tajmir-Riahi, H. A. The Role of Polymer Size and Hydrophobic End-Group in PEG-Protein Interaction. *Colloids Surf. B Biointerfaces* **2015**, *130*, 141−148.

(29) Cheng, X.; Li, M.; Wang, H.; Cheng, Y. All-Small-Molecule Dynamic Covalent Gels with Antibacterial Activity by Boronate-Tannic Acid Gelation. *Chin. Chem. Lett.* **2020**, *31* (3), 869−874.

(30) Korsmeyer, R. W.; Gurny, R.; Doelker, E.; Buri, P.; Peppas, N. A. Mechanisms of Solute Release from Porous Hydrophilic Polymers. *Int. J. Pharm.* **1983**, *15* (1), 25−35.

(31) Peppas, N. A. Analysis of Fickian and Non-Fickian Drug Release from Polymers. *Pharm. Acta Helv.* **1985**, *60* (4), 110−111.

(32) Wind, M. M.; Lenderink, H. J. W. A Capacitance Study of Pseudo-Fickian Diffusion in Glassy Polymer Coatings. *Prog. Org. Coat.* **1996**, *28* (4), 239−250.

(33) Rogers, C. E. Permeation of Gases and Vapours in Polymers. In *Polymer Permeability*; Comyn, J., Ed.; Springer Netherlands: Dordrecht, 1985; pp 11−73.

(34) Crank, J. *The Mathematics of Diffusion*; Oxford Science Publications; Clarendon Press, 1979.

(35) Wang, M. O.; Etheridge, J. M.; Thompson, J. A.; Vorwald, C. E.; Dean, D.; Fisher, J. P. Evaluation of the in Vitro Cytotoxicity of Cross-Linked Biomaterials. *Biomacromolecules* **2013**, *14* (5), 1321−1329.

(36) Poltue, T.; Karuna, C.; Khrueaduangkham, S.; Seehanam, S.; Promoppatum, P. Design Exploration of 3D-Printed Triply Periodic Minimal Surface Scaffolds for Bone Implants. *Int. J. Mech. Sci.* **2021**, *211*, 106762.

(37) Suneetha, M.; Rao, K. M.; Han, S. S. Mussel-Inspired Cell/Tissue-Adhesive, Hemostatic Hydrogels for Tissue Engineering Applications. *ACS Omega* **2019**, *4* (7), 12647−12656.

(38) Chiang, C.-W.; Chen, C.-H.; Manga, Y. B.; Huang, S.-C.; Chao, K.-M.; Jheng, P.-R.; Wong, P.-C.; Nyambat, B.; Satapathy, M. K.; Chuang, E.-Y. Facilitated and Controlled Strontium Ranelate Delivery Using GCS-HA Nanocarriers Embedded into PEGDA Coupled with Decortication Driven Spinal Regeneration. *Int. J. Nanomed.* **2021**, *16*, 4209−4224.

(39) Zhang, Y.; Huo, M.; Zhou, J.; Zou, A.; Li, W.; Yao, C.; Xie, S. DDSolver: An Add-In Program for Modeling and Comparison of Drug Dissolution Profiles. *AAPS J.* **2010**, *12* (3), 263−271.

(40) Yang, S.; Leong, K.-F.; Du, Z.; Chua, C.-K. The Design of Scaffolds for Use in Tissue Engineering. Part I. Traditional Factors. *Tissue Eng.* **2001**, *7* (6), 679−689.

(41) Li, J.; Chen, M.; Fan, X.; Zhou, H. Recent Advances in Bioprinting Techniques: Approaches, Applications and Future Prospects. *J. Transl. Med.* **2016**, *14* (1), 271.